

TUM/T39-96-12

Februar 1996

# MC simulation of vector boson production in polarized proton collisions

A. Saalfeld<sup>a,b</sup> and A. Schäfer<sup>b</sup>

<sup>a</sup> *Physik Department, Technische Universität München, D-85747 Garching, Germany*

<sup>b</sup> *Institut für theoretische Physik, Universität Frankfurt, D-60054 Frankfurt am Main, Germany*

## Abstract

We present a Monte Carlo (MC) study of  $W^\pm$  and  $Z_0$  production of longitudinally polarized proton collisions at a center of mass (CMS) energy of 500 GeV. All results were obtained with the SPHINX MC code. We consider two different types of polarized parton distributions with large and small gluon polarization. Various spin asymmetries are found to be sensitive to the shape of the polarized gluon distribution between  $0.1 \lesssim x \lesssim 0.5$ . The asymmetries are approximately constant with respect to the transverse momentum carried by the  $W^\pm$  and  $Z_0$ , *except* if the first moment of the gluon polarization is large. In this case some  $W^\pm$  asymmetries show a significant variation with transverse momentum.

PACS numbers: 13.60Hb, 13.88.+e, 14.20.Dh

Submitted to *Phys.Rev.D*

Typeset using REVTeX

## I. INTRODUCTION

In the past few years polarized deep inelastic scattering became a very attractive topic in high-energy physics. Experimentally, an important advance has been the measurement of the structure function  $g_1^p$  of the proton with high statistics [1,2]. On the theoretical side much effort has been done to decompose  $g_1^p$  into parton distributions, but the situation is still unclear (see, e.g., [3] for a recent review). This is especially true for the polarization of the sea quarks, the polarization of the gluons, the shape of the parton distributions at intermediate Bjørken  $x$ , and the small- $x$  behavior of the parton distributions.

There are in principle means to calculate all these quantities either from QCD sum rules or from lattice QCD. It will be exciting to compare future calculations and experiments.

Meanwhile the parton distributions are constructed from models of the nucleon, e.g., from Carlitz-Kaur type models [4] and many others. An even more heuristic way to obtain the parton distributions is simply to assume a generic shape of the polarized distributions and fit the strength and size parameters to the  $g_1$  data. This procedure is of course in no way unique. Many of these distributions are motivated from properties of the unpolarized distributions at larger  $x$ . Some fits invoke an SU(3) symmetric polarized sea in order to fit the first moments of the parton distributions in terms of  $\beta$ -decay and hyperon decay matrix elements, see, e.g., [5].

The naive way of comparing model parton distributions with parton distributions defined through expectation values of field theoretic operators has been much criticized [6,7]. It has been argued that a proper comparison can only be made after the axial anomaly has been taken into account which shifts the first moments of the naive parton distributions against the first moments of the field theoretic parton distributions by

$$\Delta q_f = \tilde{\Delta} q_f - \frac{\alpha_s}{2\pi} \Delta g, \quad (1)$$

where  $\Delta q_f$  denotes the field theoretic distribution of a quark with flavor  $f$  and  $\tilde{\Delta} q_f$  denotes the corresponding quantity within a quark model.  $\Delta g$  is the first moment of the polarized

gluon distribution. Equation (1) is valid for any light quark flavor  $f$ . This equation is special for longitudinal polarization. Analyzing the data within a quark model, one has to fix the four unknown quantities  $\tilde{\Delta}u$ ,  $\tilde{\Delta}d$ ,  $\tilde{\Delta}s$ , and  $\Delta g$ , neglecting the contribution of heavy quarks. But even when assuming an  $SU(3)$  symmetric sea quark distribution, the  $g_1$ ,  $\beta$ -decay, and hyperon decay experiments only fix three out of the four unknown first moments. The shapes of the distributions are of course not known at all from these considerations.

Therefore other experiments have been proposed to complement the measurement of  $g_1$  of the proton. The most important ones being semi-inclusive deep inelastic scattering [8] and polarized proton scattering [9,10]. In the present work we concentrate on proton scattering. The production of large transverse momentum photons in polarized proton collisions might be a suitable observable, but there is a large background from pion decays in the final state, as was investigated in detail in ref. [11]. This is not so for  $W^\pm$  and  $Z_0$  production at RHIC where the background from other events will be very small [9]. The limiting factor in this experiment will be the number of  $W^\pm$  and  $Z_0$  that can be produced. There are at least three different poorly known properties of the partons, which must be entangled in future experiments, namely, the amount of flavor breaking in the sea quark distribution, the size of the gluon distribution, and the shape of all these distributions. In this paper we only consider two different parametrizations. The first parametrization stems from a Carlitz-Kaur type constituent quark model with a polarized gluon, radiatively generated sea quarks starting from  $Q^2 = 10 \text{ GeV}^2$ , and a slightly broken  $SU(2) \times SU(3)$  symmetry [4]. This model does not use the anomaly equation (1), but rather identifies  $\Delta q_f$  with  $\tilde{\Delta}q_f$ . This can be justified a posteriori because in this model the gluon polarization  $\Delta g = 0.262$  turns out to be small. The interesting feature of these distributions is that they satisfy the Bjørken sum rule *and* the Ellis-Jaffe sum rule.

The other parton distributions have been taken from ref. [5]. These distributions also have  $SU(3)$  symmetric sea quarks, but the sea quarks are somewhat stronger polarized due to the lower starting point  $Q^2 = 4 \text{ GeV}^2$  of the evolution. The analysis in ref. [5] proceeds via the anomaly equation (1) and a larger ratio  $F/D = 0.590$ . Therefore, a much larger

gluon polarization of  $\Delta g = 1.971$  at  $Q^2 = 4 \text{ GeV}^2$  is obtained. The basic question we want to discuss is: Can one distinguish between these parametrizations in a  $W^\pm/Z_0$  experiment, e.g., at RHIC?

The measurement of the flavor breaking in the sea quark distribution by studying  $W^\pm$  and  $Z_0$  production is not addressed in this paper. A discussion of this interesting subject can be found in ref. [12].

The paper is organized as follows. In section II we give a very brief review of the SPHINX MC code [11,13], in which the electroweak matrix elements have now been included. In section III we present the parton distributions that are used in our MC simulation. Finally, in section IV we present and discuss the results.

## II. THE MONTE CARLO PROGRAM SPHINX

The application of perturbative QCD to Drell-Yan like reactions is complicated through the possible emission of soft and collinear radiation of partons in the initial and final state. The importance of these bremsstrahlung effects is seen most clearly from the experimental transverse momentum spectra of  $W^\pm$  and  $Z_0$  production cross sections. These spectra cannot be explained through an intrinsic transverse momentum of the initial partons. We must rather think of the transverse momentum as being generated by bremsstrahlung effects. It is not possible to calculate the K-factor exactly to arbitrary order  $\alpha_s$ , so at some stage one must rely on approximations.

The MC generator SPHINX [11], which is an extension of the well-known PYTHIA 5.6 MC code [14], treats parton radiation in leading logarithmic approximation (LLA). This means that it resums the planar bremsstrahlung graphs in an axial gauge. These graphs are exactly the universal bremsstrahlung contributions that do not depend on the particular process, e.g.,  $u\bar{d} \rightarrow W^+$  or  $u\bar{u} \rightarrow \gamma/Z_0$ . In SPHINX and PYTHIA the bremsstrahlung cascade is resummed in backwards direction, starting from the most virtual partons immediately before the reaction takes place. The longitudinal momenta of the mother partons are reconstructed

using first order polarized GLAP equations and evolved parton distributions. All information from the GLAP equation necessary to reconstruct the longitudinal momenta of the mother partons is contained in the inverse Sudakov-like formfactor

$$S_{b,h_b}(x, t_<, t_>) = \exp \left( - \int_{t_<}^{t_>} dt' \frac{\alpha_s(t')}{2\pi} \sum_{a,h_a} \int \frac{dx'}{x'} \frac{x' f_{a,h_a}(x', t')}{x f_{b,h_b}(x, t')} P_{a,h_a \rightarrow b,h_b,c,h_c}(x') \right), \quad (2)$$

giving the probability that the parton remains at  $x$  from  $t_> = \ln(Q_>^2/\Lambda^2)$  to  $t_< = \ln(Q_<^2/\Lambda^2)$ , where  $Q_<^2$  and  $Q_>^2$  denote the virtualities of the daughter and mother partons respectively. The indices  $a$  and  $b$  denote the flavors of the partons and  $h_a$  and  $h_b$  their helicities. The polarized splitting functions  $P_{a,h_a \rightarrow b,h_b,c,h_c}(z)$  can be found in ref. [15]. As it stands, the integrals diverge for the emission of soft radiation due to the poles in the splitting functions. To cure this, the soft region in the integral is cut out and treated separately. This causes no problem [14]. Note, that SPHINX cannot evolve parton distributions but rather needs evolved partons as can be seen from equation (2). For the leading-order GLAP evolution we used the code developed by Gehrmann and Stirling [5].

The full four-momenta of the mother partons can be reconstructed recursively: Consider two partons with four-momenta  $p_1, p_2$ , and virtualities  $Q_1^2 = -p_1^2$  and  $Q_2^2 = -p_2^2$  in their common CMS frame. Let  $Q_1^2 > Q_2^2$ . Then the momentum of the mother parton 3 of parton 1 is reconstructed while parton 2 is not changed. Finally, parton 3 and parton 2 are boosted to their common CMS frame and the procedure starts again until both partons have a virtuality smaller than 1 GeV.

As is well known, the variables  $x$  used in the splitting functions and in the parton distributions have no unique kinematical interpretation in LLA, see, e.g., [16]. For technical reasons in SPHINX the same prescription as in PYTHIA is used, namely, the  $\hat{s}$ -approach where  $\hat{s} = x_1 x_2 s$  is the momentary CMS energy of two partons at any stage of the evolution and  $s$  denotes the overall CMS energy of the reaction.

The last ingredients to be specified are the hard scattering cross sections. At low transverse momentum a weak boson is produced through a simple Breit-Wigner resonance. In SPHINX the treatment of the  $s$ -dependent width of the resonance is the same as in PYTHIA 5.6. We

simply use that the polarized hard scattering cross sections are related to the unpolarized ones by

$$\hat{\sigma}_{W^\pm}(\hat{s}, h_1, h_2) = \frac{1}{2} \delta_{h_1 h_2, -1} \hat{\sigma}_{W^\pm}^{unpol}(\hat{s}), \quad (3)$$

where  $h_1$ , and  $h_2$  are the helicities of the quark and antiquark respectively. A similar relation is true for  $Z_0$  production

$$\hat{\sigma}_{Z_0}(\hat{s}, h_1, h_2) = \delta_{h_1 h_2, -1} \left\{ \delta_{h_1, +1} \frac{C_L^2}{C_L^2 + C_R^2} + \delta_{h_1, -1} \frac{C_R^2}{C_L^2 + C_R^2} \right\} \hat{\sigma}_{Z_0}^{unpol}(\hat{s}) \quad (4)$$

with  $C_L = g_v + g_a$  and  $C_R = g_v - g_a$  expressed through the axial and vector coupling constants  $g_a$ , and  $g_v$  respectively. If the transverse momenta of the vector bosons become large the collinear approximation in the treatment of initial state radiation becomes bad and one should use higher order matrix elements in combination with the radiation algorithm. For this purpose we implemented the next-to-leading order QCD and QED polarized cross sections in SPHINX. The QCD cross sections can be found in ref. [17] but we also list them here: The annihilation process  $q(h_1) + \bar{q}(h_2) \rightarrow g + Vectorboson$  has to lowest order in  $\alpha_s$  the scattering cross section

$$\frac{d\hat{\sigma}_{q(h_1), \bar{q}(h_2)}}{d\hat{t}} = \frac{2}{9} \alpha_s (b - h_1 a)^2 (1 - h_1 h_2) \frac{1}{\hat{s}^2} \left( \frac{\hat{u}}{\hat{t}} + \frac{\hat{t}}{\hat{u}} + \frac{2M_V^2 \hat{s}}{\hat{t} \hat{u}} \right). \quad (5)$$

The QCD Compton process  $q(h) + g(\lambda) \rightarrow q + Vectorboson$  has in leading order  $\alpha_s$  the cross section

$$\frac{d\hat{\sigma}_{q(h), g(\lambda)}}{d\hat{t}} = -\frac{1}{12} \alpha_s (b - h a)^2 \frac{1}{\hat{s}^2} \left\{ (1 + \lambda h) \left( \frac{\hat{s}}{\hat{t}} + \frac{\hat{t}}{\hat{s}} + \frac{2M_V^2 \hat{u}}{\hat{t} \hat{s}} \right) - 2\lambda h \frac{(M_V^2 - \hat{t})^2}{\hat{t} \hat{s}} \right\}. \quad (6)$$

Here  $h_1, h_2, h (= \pm 1)$ , and  $\lambda (= \pm 1)$  denote the incoming parton helicities. For  $Z_0$  production one has to substitute

$$\begin{aligned} a_u &= -a_d = \frac{g}{4\cos\theta_W}, \\ b_u &= \frac{g}{4\cos\theta_W} \left( -1 + \frac{8}{3} \sin^2\theta_W \right), \\ b_d &= \frac{g}{4\cos\theta_W} \left( 1 - \frac{4}{3} \sin^2\theta_W \right), \end{aligned} \quad (7)$$

for  $a$  and  $b$ , where  $g = e/\sin\theta_W$ . In the case of  $W^\pm$  production one has to substitute

$$\begin{aligned} a_{ud} = b_{ud} &= -\frac{g}{2\sqrt{2}}\cos\theta_C, \\ a_{us} = b_{us} &= -\frac{g}{2\sqrt{2}}\sin\theta_C, \end{aligned} \quad (8)$$

for  $a$  and  $b$ , where  $\theta_C$  is the Cabibbo angle.

### III. THE PARTON DISTRIBUTIONS

In this section we describe the main physics properties of the parton distributions that we used in the simulation. For details see refs. [4] and [5]. These parton distributions have been slightly modified because we use different unpolarized parton distributions in both cases. We have taken those from Glück et al. [18]. If the helicity distributions are required to be positive, the absolute value of the polarized distributions cannot be larger than the unpolarized ones, viz.

$$f_\pm(x) = \frac{1}{2}(f(x) \pm \Delta f(x)) > 0 \Rightarrow |\Delta f(x)| \leq f(x) \quad (f = q, g). \quad (9)$$

Whenever  $|\Delta f(x)|$  gets larger than  $f(x)$  we substitute it by  $|\Delta f(x)| = f(x)$ . This modifies the parton distributions a little bit at large  $x$  as can be seen from fig. 2.

The first parametrization of the polarized parton distributions [4] is based on a Carlitz-Kaur type spin-dilution model for the proton's distribution functions. It is referred to as CKT. The important aspects of this model are:

- The gluon distribution can be expressed through the valence quarks because of the spin-dilution idea.
- It uses a non-standard ratio of the SU(3) coupling constants  $F/D = 0.49 \pm 0.08$ .
- The free parameters of the model are chosen to fulfill the Bjørken and Ellis-Jaffe sum rule which turns out to be possible due to the above non-standard  $F/D$  ratio.

- The fit to the  $g_1(x, Q^2)$  data is made at  $Q_0^2 = 10 \text{ GeV}^2$ . There are no polarized strange quarks at this  $Q^2$ .
- The first moment of the gluon distribution  $\Delta g = 0.262$  is rather small in this model. So it makes no difference if one uses the anomaly relation (1) or the naive identification.

The shape of these parton distributions can best be read off from fig. 1. They are shown in this figure for a low resolution of  $Q = 2 \text{ GeV}$  as well as for a large resolution that is approximately equal to the  $W^\pm$  mass. Note that we use  $n_f = 3$  for the number of flavors in the GLAP equation, whereas  $n_f = 2$  has been taken in ref. [4].

The second type of parton distributions, taken from [5], is a simple fit to  $g_1$  using  $\beta$ -decay and hyperon decay data to fix the first moments of the polarized distributions. For the shape of the distributions a generic function is assumed and the shape parameters are fitted to the  $g_1$  data. The important aspects of this distributions are:

- The sea is taken to be SU(3) flavor symmetric and vanishes at  $Q_0^2 = 4 \text{ GeV}^2$ .
- The gluon polarization  $\Delta g = 1.971$  is rather large, mainly due to the larger value  $F/D = 0.590$  and the anomaly equation (1).
- Three different shapes of the distributions are considered. They all fit the data equally well. These parton distributions are called SETA, SETB, and SETC.

The shapes of the the distributions can be read off from fig. 2. It can also be seen from this figure that the valence quarks in both parton distributions are quite similar in size and shape.

#### IV. RESULTS

Before showing our results, we have to fix some notation and introduce the spin asymmetries. By  $(s_1, s_2)$ ,  $s_1, s_2 = \pm$ , we will denote a *spin* configuration of the scattering protons.  $s_1 = +$  means that the proton which moves in the direction of the positive z-axis has a spin

that also points in the  $z$ -direction.  $s_1 = -1$  means that the spin of this proton points in the negative  $z$ -direction. The spin of this particle is by convention equal to its helicity. The spin of the other proton is denoted by  $s_2$ . Note that its helicity is always opposite to its spin, e.g.,  $(+, +)$  means that the ‘beam proton’ has spin and helicity  $+$ , whereas the ‘target proton’ has spin  $+$  and helicity  $-$ .

By a  $2 \rightarrow 1$  process we mean resonance production through a hard scattering cross sections (3), and (4). A  $2 \rightarrow 2$  process proceeds by definition through the annihilation amplitude (5), or Compton amplitude (6). In both cases we generate higher order corrections through the MC algorithm explained in section II. This means in particular that  $2 \rightarrow 1$  processes together with radiation contain those parts of  $2 \rightarrow 2$  processes that survive the LLA. Therefore, one should switch on either  $2 \rightarrow 1$  processes or  $2 \rightarrow 2$  process, not both. For large transverse momenta  $2 \rightarrow 2$  processes must be used because they describe the emission of an additional parton more accurately. On the other hand, if the transverse momentum is low, not any event is accompanied by an additional parton radiation and one should switch to the  $2 \rightarrow 1$  processes. If we compare the cross sections, we find that the switch from  $2 \rightarrow 1$  to  $2 \rightarrow 2$  processes should be made for transverse momenta of about  $p_T = 4$  GeV. The same  $p_T$  is obtained by comparing the asymmetries derived from  $2 \rightarrow 1$  and  $2 \rightarrow 2$  processes. After these preliminary remarks we define the asymmetries and show the results. The parity conserving asymmetry is defined through

$$A_{LL}^{PC} = \frac{(+ -) + (- +) - (+ +) - (- -)}{(+ -) + (- +) + (+ +) + (- -)}. \quad (10)$$

We consider three different parity violating asymmetries, namely,

$$A_{LL}^{PV1} = \frac{(+ -) - (- +)}{(+ -) + (- +)}, \quad (11)$$

$$A_{LL}^{PV2} = \frac{(- +) - (- -)}{(- +) + (- -)}, \quad (12)$$

$$A_{LL}^{PV3} = \frac{(- -) - (+ -)}{(- -) + (+ -)}. \quad (13)$$

A test asymmetry

$$A_{LL}^{TEST} = \frac{(++) - (--)}{(++) + (--)}, \quad (14)$$

which vanishes trivially from rotation invariance, shows the quality of the calculation.

The spin-asymmetries are plotted in figs. 3, 4, and 5 against the transverse momentum of the vector bosons in the CMS frame of the reaction. For each orientation of the protons, 0.1 million events have been produced <sup>1</sup>. This is a roughly realistic number for the RHIC spin experiment with a luminosity of  $10^{32}/cm^2s$  and 1.5 years of running. Some asymmetries are quite sensitive to the structure functions. But one must be careful not to attribute this to the *size* of the polarized gluon distribution alone. First of all, one can see from the asymmetries corresponding to SETA, SETB, and SETC, which only differ by the shape of the gluon distribution, that the magnitude of the asymmetries is quite sensitive to the *shape* of  $\Delta g$ . See fig. 3 and note that all Gehrmann/Stirling distributions (full symbols) have the same  $\Delta g$  but give very different asymmetries. These asymmetries overlap with those obtained for the CKT distributions (open circles), which have much smaller  $\Delta g$ . Interestingly, there is another significant distinction between the distributions with small and large  $\Delta g$ : Some asymmetries derived from SETA, SETB, and SETC vary significantly with transverse momentum  $p_T$ , whereas those derived from the CKT distributions stay approximately constant. One can see this most clearly from the parity violating asymmetries  $A_{LL}^{PV2,W^+}$  and  $A_{LL}^{PV3,W^-}$ . This effect can be traced back to the hard scattering cross sections eqns. (5), and (6). Even though the Compton process is suppressed by a factor of 3/8, it can become comparable to the annihilation process for large transverse momenta because the Compton scattering falls off less rapidly than the annihilation scattering. At very large transverse momenta the Compton induced asymmetry will saturate the spin asymmetry. Fig. 6 shows that the transition region from an annihilation induced asymmetry to a Compton induced asymmetry

---

<sup>1</sup>This requires about 3 hours of CPU time for one spin orientation on an IBM-RISC6000 workstation.

can be reached for the distribution SETB (and as well for SETA, and SETC). This is not possible for the CKT distribution, at least up to  $p_T \approx 20$  GeV. The transition can also be observed in the corresponding spin asymmetry fig. 7. Finally, one can see from fig. 8 that the range in  $x$  where the cross section is large lies approximately between  $0.1 \lesssim x \lesssim 0.5$  with a strong maximum at about  $x = 0.1$ .

## V. CONCLUSIONS

We have presented an extension of the MC generator SPHINX to polarized  $W^\pm$  and  $Z_0$  production. Using two different types of parton distributions in a MC simulation at  $\sqrt{s} = 500$  GeV, we find that several details of the calculated asymmetries show an unexpected sensitivity to the polarized parton distributions. The variation of the spin asymmetries  $A_{LL}^{PV2,W^+}$  and  $A_{LL}^{PV3,W^-}$  with transverse momentum  $p_T < 20$  GeV are especially interesting. The upper limit in  $p_T$  in our simulation is dictated by MC statistics. For  $p_T > 4$  GeV we use NLO hard scattering cross sections in combination with initial state radiation. The simulations show that not only the size but also the  $p_T$  dependence of some asymmetries is sensitive to  $\Delta g$ . To make use of this information, one has to measure the total  $p_T$  of the hadronic products in addition to the charged lepton from the  $W^\pm$  decay.

We only showed results for the transverse momentum spectra because they are especially interesting for measuring the polarized gluon distribution. There many other important observables that can be generated by SPHINX. Rapidity distributions, for example, are sensitive to flavor asymmetries in the polarized sea quark distribution.

## ACKNOWLEDGMENTS

We thank B. Ehrnsperger, S. Güllenstern, L. Mankiewicz, and E. Stein for illuminating discussions, and S. Gehrmann for providing us with his parton distributions. A. Schäfer acknowledges support by DFG (G. Hess Programm), BMBF, and MPI für Kernphysik (Heidelberg).

## REFERENCES

- [1] J.Ashman *et al.*, Phys. Lett. **B 206**, 364, (1988).
- [2] D.Adams *et al.*, Phys. Lett. **B 329**, 399, (1994).
- [3] M.Anselmino, A.Efremov, and E.Leader, Phys. Rep. **261**, 1–124, (1995).
- [4] B. Ehrnsperger, A. Schäfer, Phys. Rev. D **52**, 2709, (1995).
- [5] T.Gehrman and W.J.Stirling, Z. Phys. C **65**, 461, (1995).
- [6] R.D.Carlitz, J.C.Collins, and A.H.Mueller, Phys. Lett **B 214**, 229, (1988).
- [7] L.Mankiewicz and A.Schäfer, Phys. Lett. **B 242**, 455, (1990).
- [8] S.Güllenstern, M.Veltri, P.Górnicki, L.Mankiewicz, and A.Schäfer, Phys. Lett. **B 312**, 166, (1993).
- [9] RHIC Spin-Collaboration, *Proposal on Spin Physics Using the RHIC Polarized Collider*, 1992.
- [10] RHIC Spin-Collaboration, *Proposal on Spin Physics Using the RHIC Polarized Collider - Update*, 1993.
- [11] S.Güllenstern, Nucl. Phys. **A560**, 494, (1993).
- [12] C.Bourrely, J.Soffer, Nucl. Phys. **B423**, 329, (1994).
- [13] S.Güllenstern, Dissertation, Universität Frankfurt am Main, 1994.
- [14] T. Sjöstrand, M. Bengtsson, and M. van Zijl, Z. Phys. C **32**, 67, (1986).
- [15] G.Altarelli and G.Parisi, Nucl. Phys. **B126**, 298, (1977).
- [16] Y.L.Dokshitzer, D.I.Dyakonov, and S.I.Troyan, Phys. Rep. **58**, 269-395, (1980).
- [17] K.Hidaka, Nucl. Phys. **B192**, 369, (1981).
- [18] M.Glück, E.Reya, and A.Vogt, Z. Phys. C **48**, 471, (1990).

## FIGURES

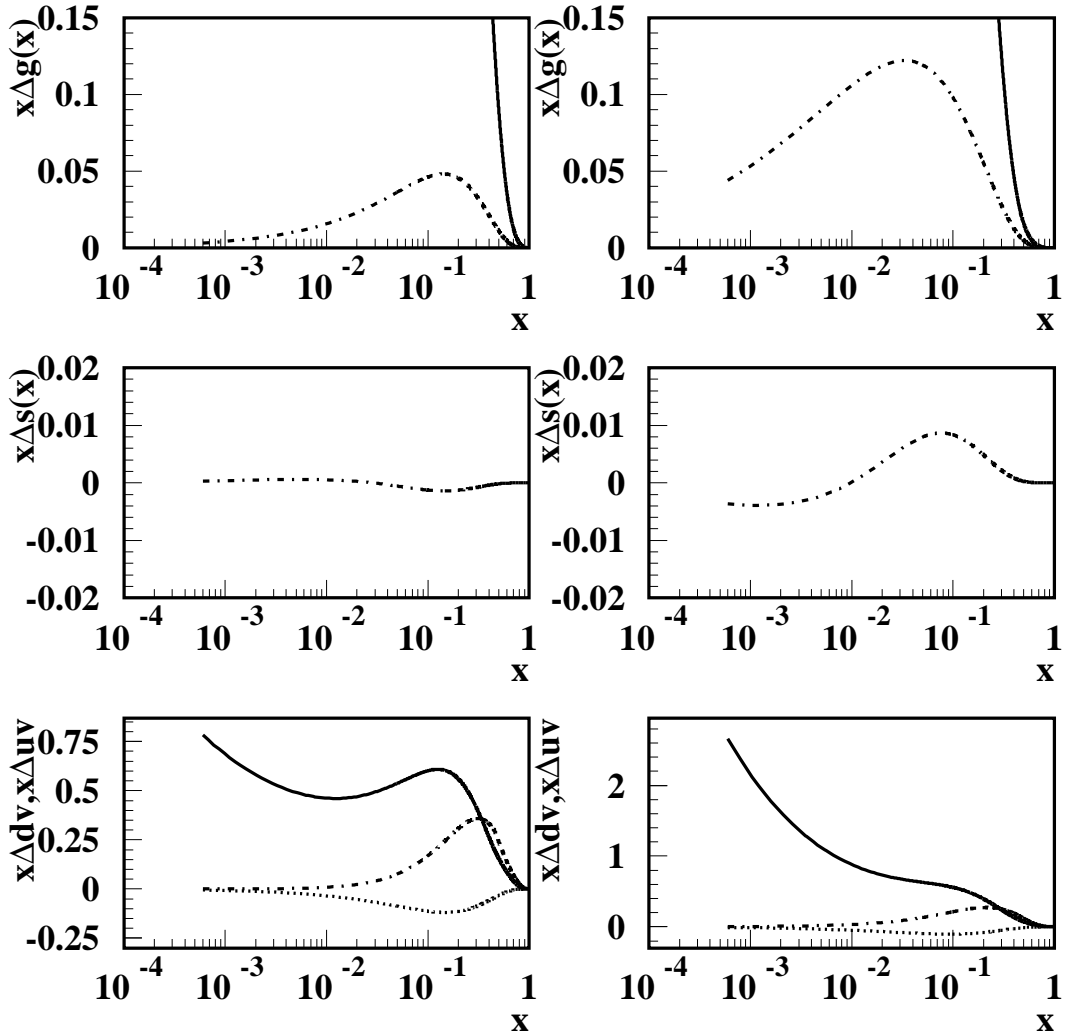


FIG. 1. MC reconstruction of the CKT parton distribution with SPHINX at  $Q^2 = 4 \text{ GeV}^2$  (left), and  $Q^2 = 8100 \text{ GeV}^2$  (right). For comparison, also the unpolarized quantities are shown (solid lines).

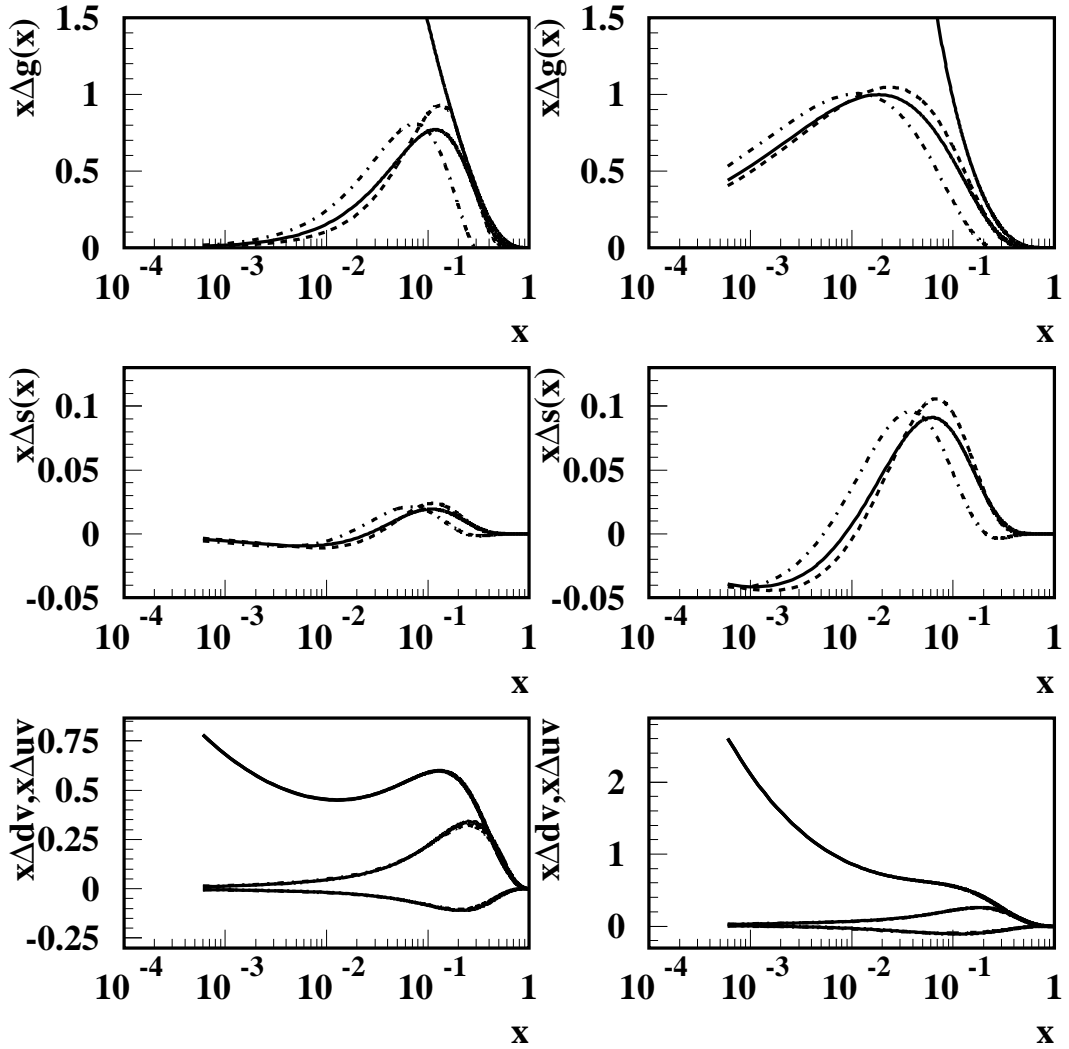


FIG. 2. MC reconstruction of the parton distributions SETA, SETB, and SETC with SPHINX at  $Q^2 = 4 \text{ GeV}^2$  (left), and  $Q^2 = 8100 \text{ GeV}^2$  (right). Solid lines show the SETA distributions, dashed lines SETB, and dash-dotted lines SETC. For comparison, also the unpolarized quantities are shown (solid line).

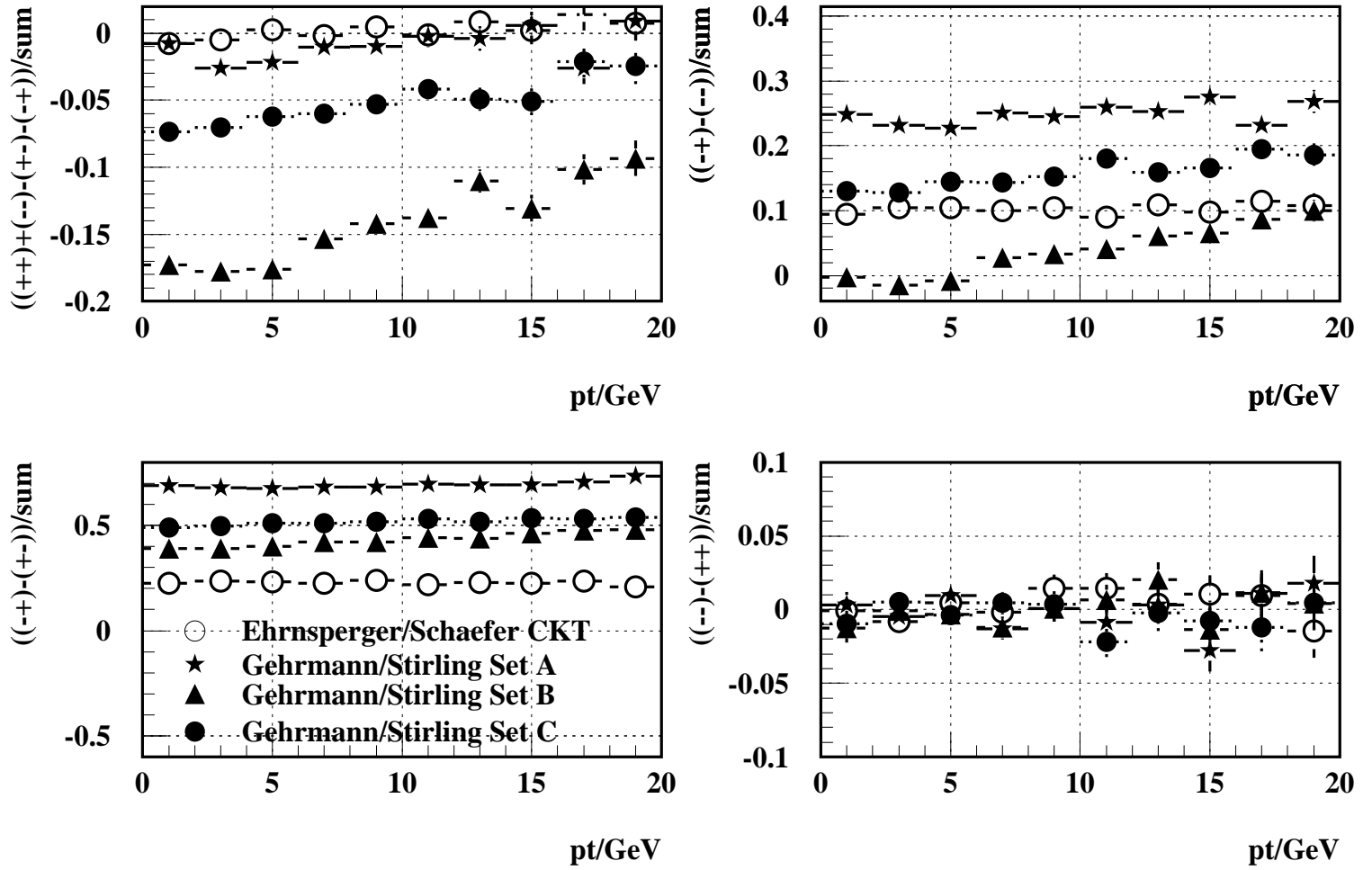


FIG. 3. Transverse momentum distributions of the spin asymmetries defined in eqns. (10), (11), (12), and (13) for  $W^+$ -production  $2 \rightarrow 2$  processes and SETA, SETB, SETC, and CKT partons.

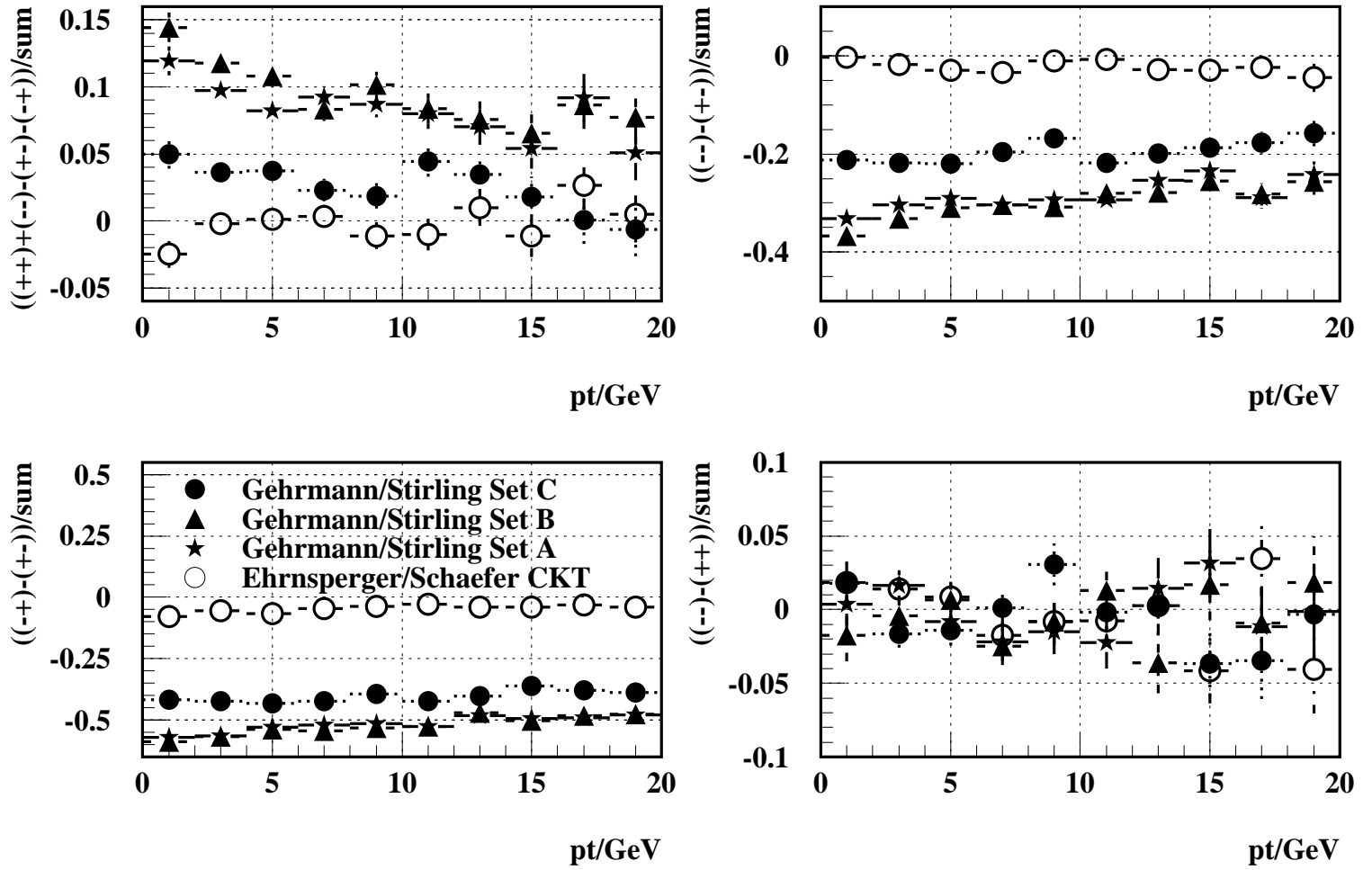


FIG. 4. Transverse momentum distributions of the spin asymmetries defined in eqns. (10), (11), (12), and (13) for the  $W^-$ -production  $2 \rightarrow 2$  processes and SETA, SETB, SETC, and CKT partons.

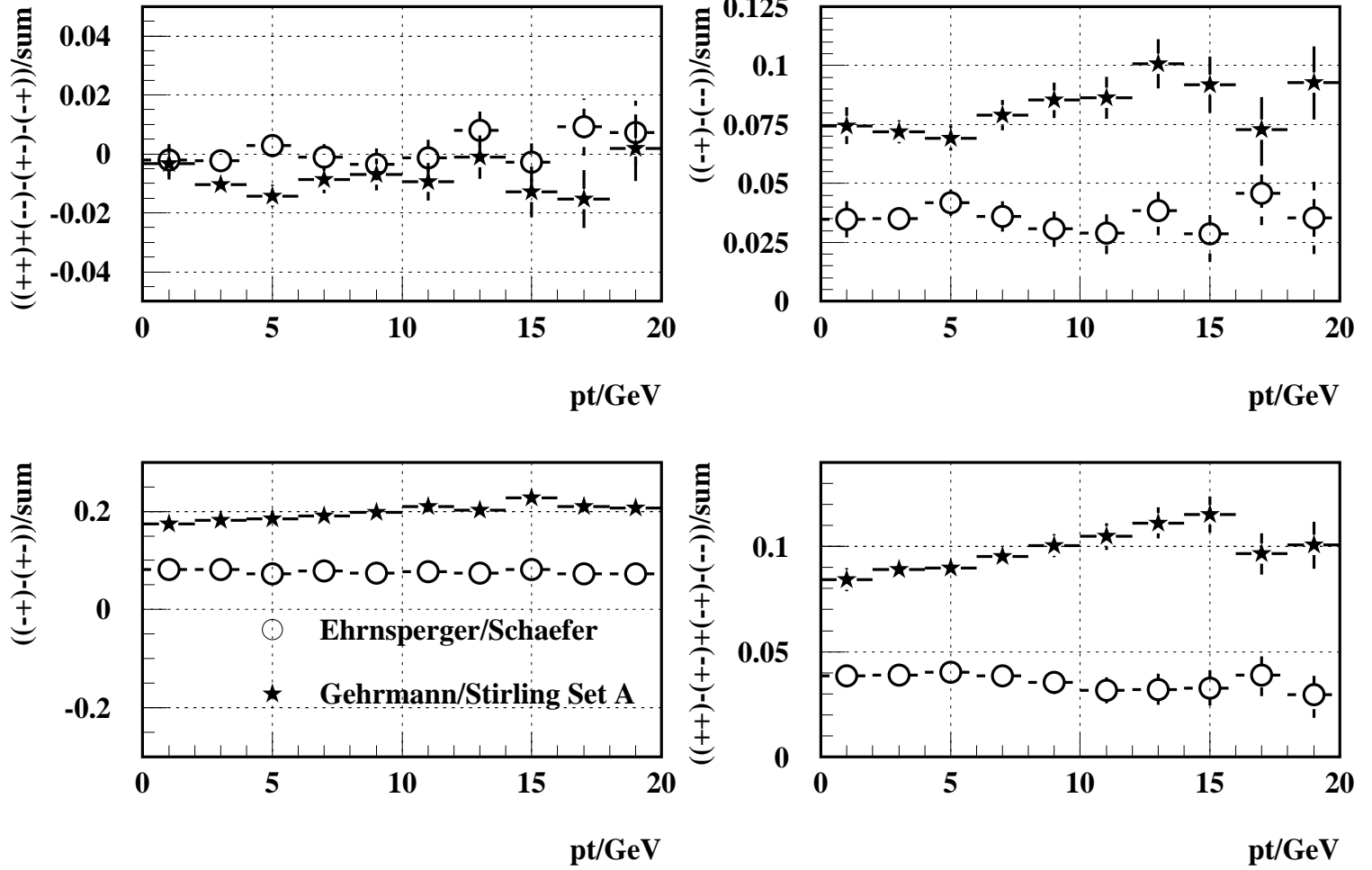


FIG. 5. Transverse momentum distributions of the spin asymmetries defined in eqns. (10), (11), (12), and (13) for the  $Z_0$ -production  $2 \rightarrow 2$  processes and SETA and CKT partons.

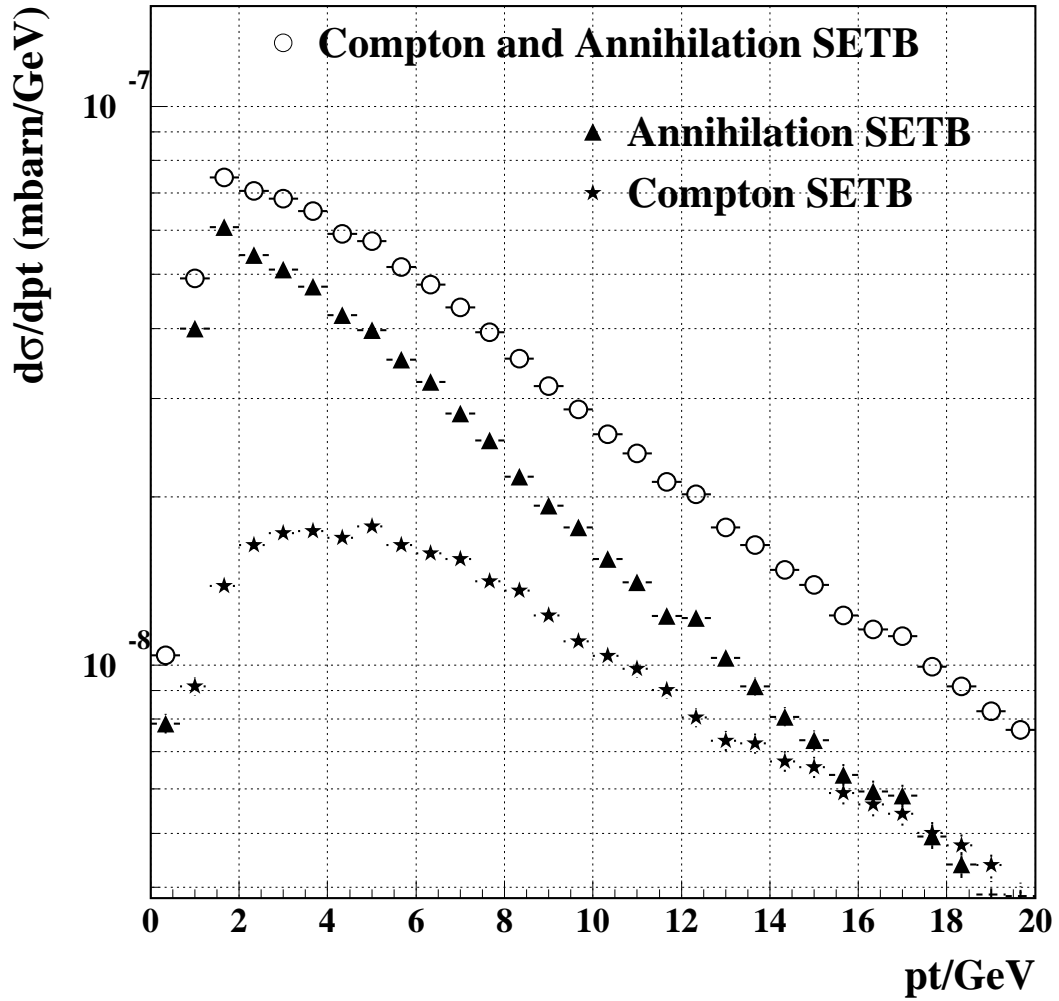


FIG. 6. Contributions to the transverse momentum distribution of  $W^+$ 's for a spin orientation  $(-+)$  of the protons and SETB partons. This spin orientation gives the largest ratio of Compton to annihilation scattering.

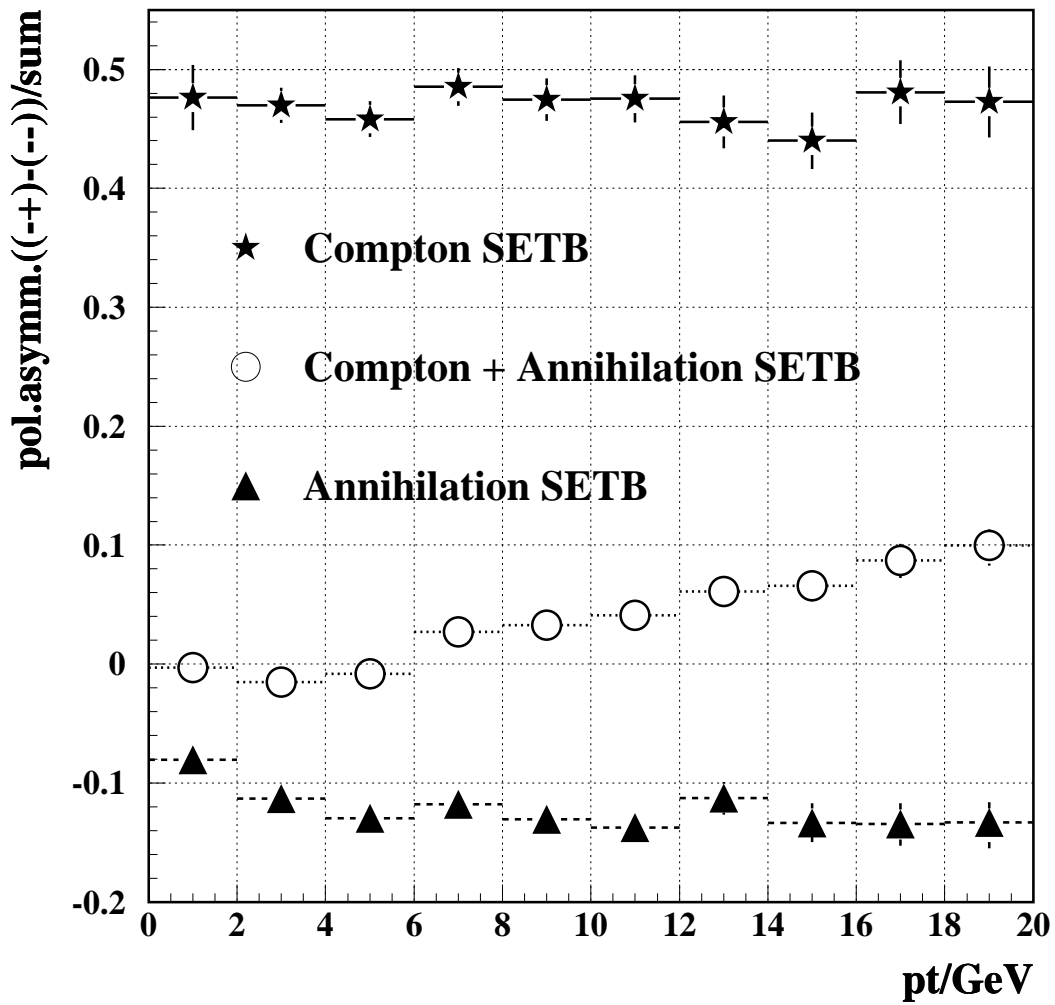


FIG. 7. Contributions to the asymmetry  $A_{LL}^{PV2}$  in  $W^+$  production for SETB partons.

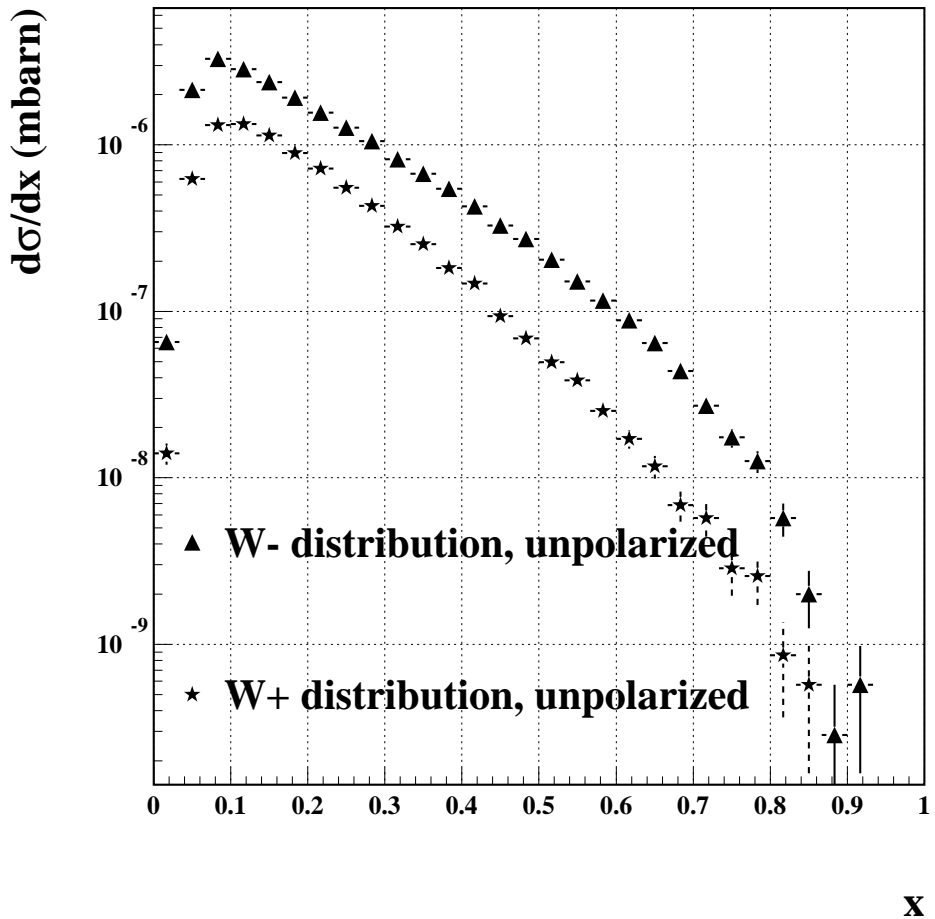


FIG. 8. The  $x$  distribution of  $W^\pm$ 's for unpolarized proton scattering at  $\sqrt{s} = 500$  GeV. Only events with  $p_T > 5$  GeV have been considered.